In-plane coupling and field enhancement in infrared metamaterial surfaces

Boubacar Kanté,* André de Lustrac, and Jean Michel Lourtioz†
Institut d'Electronique Fondamentale, Université Paris-Sud, CNRS UMR 8622, Orsay F-91405, France
(Received 23 March 2009; revised manuscript received 11 June 2009; published 7 July 2009)

In-plane coupling between the second plasmonic mode of split ring resonators and delocalized plasmons of nanowires is experimentally demonstrated from far-field measurements in metasurfaces with critical separation distances between nanostructures. Near-field calculations show that coupling drastically depends on both "meta-atom" shapes and separation distances. The associated field enhancement reveals these metasurfaces as good candidates for applications to sensing and surface enhanced spectroscopy.

DOI: 10.1103/PhysRevB.80.035108 PACS number(s): 42.70.Qs

Periodic arrays of metallic split ring resonators (SRRs) and/or nanowires represent an important class of metamaterials,[1–3] and great efforts have been devoted to translating their electromagnetic properties from the microwave to the optical regime.[4,5] The majority of experimental reports have attempted to tailor the effective-medium properties (permittivity, permeability, and refractive index) in free-space configurations. Multilayer structures of SRRs and/or nanowires have thus been shown to exhibit a magnetic response at normal incidence due to coupling effects between metallic elements of adjacent layers.[6–8] In contrast, despite some investigations of in-plane coupling effects[9,10] little attention has been given to this subject in the metamaterial context mostly because reproducible fabrication of metamaterial structures with in-plane elements regularly spaced by only a few tens of nanometers is a real challenge. Specifically, proximity effects in e-beam lithography represent a major obstacle for such small spacings. It is easier to bring metallic elements close to each other in a vertical multilayer stack where adjacent metalayers are separated by thin insulator layers. However, coupling effects not only modify the electromagnetic responses of bulk metamaterial structures but also lead to dramatic enhancements of the local electromagnetic field. From this point of view, in-plane coupling is of much greater interest than vertical coupling since local-field enhancement is directly accessible by near-field microscopic techniques, resulting in possible applications in biological and chemical sensing, second-harmonic generation, and surface-enhanced spectroscopies.[11–13] In this paper, we report an experimental demonstration of in-plane coupling between nontouching metallic metamaterial "atoms" in an infrared metamaterial composed of gold SRRs and continuous nanowires deposited on a low-doped silicon substrate. Coupling effects manifest themselves as a splitting of the second plasmonic resonances of SRRs measured in the transmission spectra. Strong electromagnetic field enhancements associated with strong in-plane coupling effects reveal that metasurfaces based on SRRs and nanowires are good candidates for sensing applications.

Excitation of high-order resonances in subwavelength nanoparticles is an important issue in plasmonics. To date, most research has been directed to plasmon dots or elementary dipoles,[14] hypothetically capable of supporting high-order resonances. Recently, such resonances have been specifically investigated in structures with broken symmetry, where normally dark modes could be excited from a strong bright mode.[15,16] The originality of our work stems from the use of folded metallic elements (i.e., SRRs), whose second plasmonic mode can be easily excited by a plane wave normally incident onto the substrate. Since this mode can also efficiently couple to guided modes of continuous nanowires, combining SRRs and nanowires offers a solution for efficient excitation of guided nanowire modes from a normally incident plane wave. Nanoresonators with relatively low radiative losses such as SRRs offer indeed more flexibility than elementary dipoles or dots to mediate the coupling of external waves to nanoguides. The space between each SRR base and the nearby nanowire constitutes a region of field exaltation, which can be exploited in the design of nanosensors.

Previous investigations of the electromagnetic response of periodic arrays of SRRs have revealed two types of plasmonic modes whose field maxima and nodes depend both on the resonance order and on the symmetry of the structure with respect to light polarization.[17,18] While odd modes with an odd number of field nodes and a magnetic moment can be excited for an incident electric field parallel to the resonator gap, even modes with an even number of field nodes and an electric moment are excited for a polarization perpendicular to the gap. This classification has been verified using scanning near-field optical measurements with a simultaneous resolution of near-field magnitude and phase.[19] Strong coupling effects were numerically predicted around the second odd mode for periodic arrays of SRRs and continuous nanowires separated by a few tens of nanometers.[18] Here, we show experimentally and numerically that the coupling strength is not only related to the physical proximity of metallic elements (resonators and wires) but also to the complex distribution of field maxima and nodes over all the structures, which itself critically depends on the resonator shape. Strong coupling is accompanied by a splitting of the second SRR mode into two eigenmodes of different symmetries. While field enhancement is mainly obtained for the low-frequency antisymmetric component, the spectral separation between the two components is a measure of the optical distance between the SRR base and nearby nanowire. This can be used, for instance, in sensing or nonlinear optics applications by filling in the SRR base/nanowire interspace with molecules or active materials.

Figure 1 (top) shows the structures investigated in this work. All consist of nanoresonators and continuous nanowires, which are the basic constituents of negative refraction metamaterials.[1–3,18] The nanoresonators are either triangular,

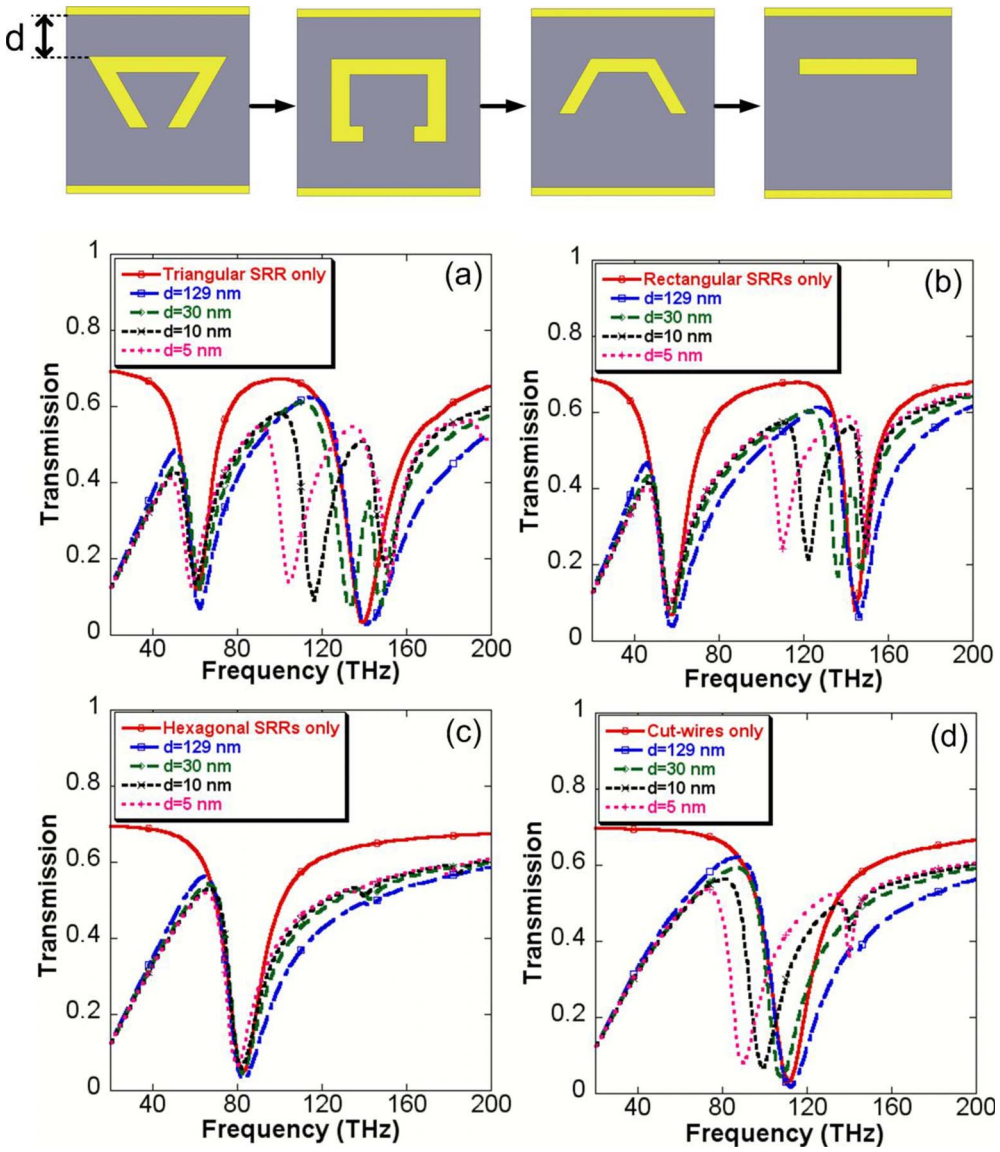

FIG. 1. (Color online) Top: unit cells of the different structures studied in this work. Bottom (a)–(c): transmission spectra calculated at normal incidence for structures with triangular, rectangular, and hexagonal SRRs, respectively. (d) transmission spectra of structures with cut-wire resonators. In all cases, continuous red curves are obtained in the absence of continuous wires. Dashed curves are for the entire structures comprised of resonators and continuous wires. The different colors correspond to different distances between the two metallic elements. A Drude model is assumed for gold (Ref. 18). The relative permittivity of silicon is taken to be 11.9. The width and height of metal stripes used for resonators and wires are 50 and 40 nm, respectively.

rectangular, and hexagonal SRRs or simple cut wires with edge angles of 60°, 90°, 120°, and 180°, respectively. Numerical simulations were performed using the finite element method (HFSS from Ansoft) for a normal-to-plane incidence of the external wave with the electric field parallel to the continuous wires and the resonator gap. In this situation, only localized plasmon modes with an odd number of nodes[17–19] can be excited in SRRs. The external light does not couple to guided modes of continuous nanowires, which act, in fact, as asymmetric plasmon guides. Figures 1(a)–1(d) (bottom) show the calculated transmission spectra. Continuous red curves are for periodic arrays of nanoresonators alone. Dashed curves are for the structures comprised of nanoresonators and continuous wires. The different colors correspond to different distances between the two metallic elements. As seen, in the spectral region of interest, periodic arrays of either triangular or rectangular SRRs exhibit two resonant modes [Figs. 1(a) and 1(b)], while only one mode, the fundamental one, is observed for periodic arrays of hexagonal SRRs [Fig. 1(c)] or cut wires [Fig. 1(d)]. Actually, the second resonance of hexagonal SRRs occurs at higher frequencies and has a much lower amplitude than in the case of other SRRs. If the distance between SRRs and continuous wires is long enough (~130 nm), the optical response of each composite structure can be qualitatively seen as the sum of two separate contributions: (1) the Drude-like optical response of the periodic array of continuous wires alone (not shown here) and (2) the optical response of metallic resonators alone [red curves in Figs. 1(a)–1(d)]. When the separation distance is drastically reduced, the transmission spectra

can strongly deviate from this superposition. In the case of triangular and rectangular SRRs [Figs. 1(a) and 1(b)], the second resonant mode splits into two components while the first mode is essentially unaltered. This first mode is less robust in the cases of hexagonal SRRs and cut wires [Figs. 1(c) and 1(d)]. The fundamental mode of cut-wire structures is first shifted to lower frequencies and then a splitting occurs for separations below 10 nm [Fig. 1(d)]. Splitting effects are the clearly signature of charge coupling effects between continuous wires and SRRs, which can be regarded as one-dimensional asymmetric plasmonic waveguides[20,21] and subwavelength nanoparticles acting as electric monopoles or multipoles,[17–19] respectively. Even though the incident plane wave cannot directly couple to the guided modes of nanowires, coupling occurs due to the broadband distribution of wave vectors "generated" from the nanoresonators.[22] It is important to note that in Figs. 1(a), 1(b), and 1(d) only the low-frequency component of the spectral doublet is shifted in frequency when decreasing the distance between SRRs and nanowires. Actually, the high-frequency component near 150 THz remains "frequency locked" onto the symmetric guided mode.[20] This component appears weakly in the transmission spectrum of the third structure for $d=5$ nm [Fig. 1(c)]. In contrast, the low-frequency component corresponds to a guided mode that is less confined in the wire and therefore more sensitive to proximity effects with the resonators.

Results of Fig. 1 clearly show that the structures can be classified into "SRR-like" ones with a second resonance of high amplitude (structures 1 and 2) and "cut-wire-like" ones (structures 3 and 4) in which the second resonance is either suppressed or has a small amplitude. Correspondingly, coupling effects in SRR-like structures are stronger than in cut-wire-like ones. Given this classification, two types of periodic structures were fabricated: (1) devices with rectangular SRRs and continuous wires and (2) ones with cut wires and continuous wires. Figure 2 (top) shows scanning electron micrographs of the fabricated structures. In the first series of samples, the distance between continuous wires and resonators was typically around 120 nm, while it was close to 30 nm in the second series of samples. For both series of samples, extreme regularity of the metallic patterns, whose period is ~600 nm, was realized. Each sample consists of 100×100 μm^2 metasurfaces, fabricated by e-beam lithography on a 280-μm-thick silicon substrate. The fabrication process thus includes e-beam lithography, high-vacuum electron-beam evaporation of 5 nm titanium, 40-nm-thick gold film, and a lift-off procedure. All structures were fabricated in a single run, thus allowing a meaningful comparison of their optical responses. The e-beam lithography was pushed to its limits for the fabrication of regular structures with very small distances between metallic elements ($d=30$ nm). The transmission spectra were measured under normal-to-plane incidence with a Fourier-transformed infrared (FTIR) spectrometer BioRad FTS 60 equipped with a Cassegrain microscope. The FTIR beam was polarized parallel to the SRR gaps (or to the wires). Measurement results are reported in Figs. 2(a) and 2(b). Curves in Fig. 2(a) were obtained for the metasurfaces with SRRs and continuous wires and for two distances between the metallic elements ($d=120$ nm, blue curve; $d=30$ nm, red curve). Curves in Fig. 2(b) were obtained for metasurfaces with cut and continuous wires and the same distances between metallic elements.

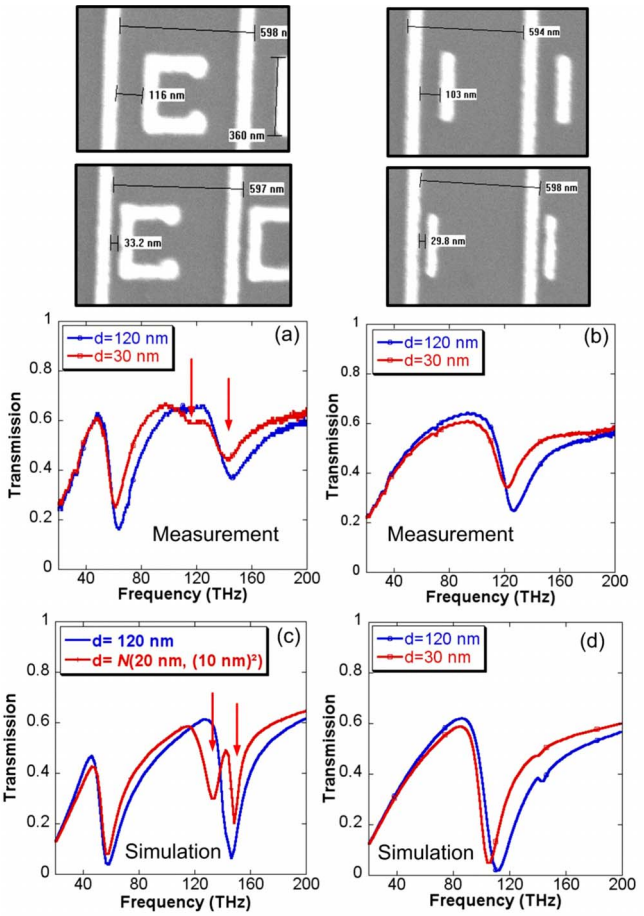

FIG. 2. (Color online) Top: scanning electron micrographs of the fabricated structures. Bottom: transmission spectra of these structures at normal incidence. (a) and (c) Measurements and calculations for the structures comprised of SRRs and wires. (b) and (d) Measurements and calculations for the structures comprised of cut and continuous wires. In each case, blue curves are obtained for a separation $d=120$ nm between resonators and continuous wire and red curves are obtained for $d=30$ nm.

In agreement with theoretical calculations of Fig. 1(b), two resonances are observed for the periodic array of rectangular SRRs and wires separated by a distance $d\sim120$ nm. Bringing SRRs closer to the continuous wires ($d\sim30$ nm) had a weak influence on the first SRR resonance at ~60 THz. This is explained by the fact that electric charges in the SRR are concentrated near the SRR gap far from the continuous wire. A different situation is observed for the second SRR resonance originally located at ~140 THz but here split into two components at ~120 and ~150 THz. For this second resonance, a large fraction of electric charges is actually concentrated in the SRR base close to the continuous wire. However, the transmission minimum corresponding to the low-frequency component of the split mode is both much broader and less pronounced than in the theoretical calculations of Fig. 1(b). Its frequency position (120 THz) would also correspond to a distance of 20 nm between metallic

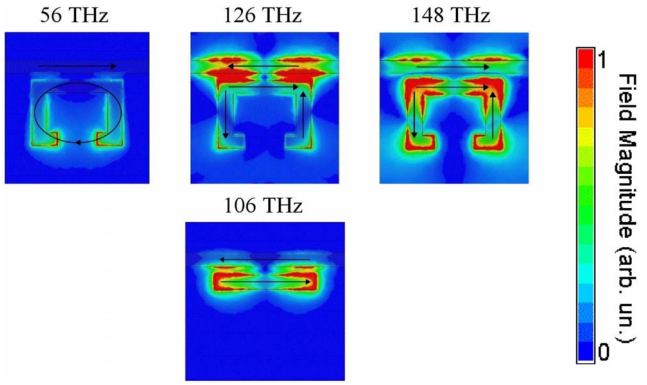

FIG. 3. (Color online) Near-field distributions calculated at the different transmission minima in Figs. 2(c) and 2(d) (total electric field intensity at the bottom surface of the metallic elements). The scale has been modified for comparison and visibility. Colors from blue to red correspond to increasing magnitude of the total electric field.

elements rather than 30 nm. Fabrication imperfections and size dispersion from one metamaterial cell to another provide in part a likely explanation for these discrepancies. This is especially pertinent because the position of the low-frequency component is very sensitive to the separation distance. Due to the Gaussian-like energy distribution of the electron beam used in lithography, the width of metallic stripes could be slightly larger than expected at the substrate/metal interface, leading in turn to a closer proximity of metallic elements. A second run of simulations was performed assuming a Gaussian distribution for the separation distance between metallic elements from one cell to another. The distribution was centered at 20 nm with a standard deviation of 10 nm. Results of these simulations are reported in Fig. 2(c), which in agreement with the experiments show a broader transmission dip with a smaller amplitude than in Fig. 1(b). Residual discrepancies can be attributed to surface roughness and dissipative losses in metal.

The measurement results for the structures with cut wires [Fig. 2(b)] are found to be in good agreement with the theoretical calculations reported in Figs. 1(d) and 2(d). Only the fundamental mode (the dipolar mode) is observed in the frequency range of measurements. Bringing cut wires closer to continuous wires ($d=30$ nm) shifts the resonance frequency from 130 to 120 THz. A mode splitting as shown in Fig. 1(d) only occurs for separation distances smaller than 20 nm. Coupling with the guided modes of nanowires is explained in this case by the presence of field maxima at the cut-wire ends, i.e., in close proximity of the nearby nanowire. Direct illustrations of coupling phenomena are obtained from calculated near-field and current distributions, as shown in Fig. 3. For the first SRR resonance (leftmost field map), there is only one field node in the SRR (Refs. 17–19) and the field intensity is concentrated near the SRR gap regardless of the distance between the SRR and nearby wire. A single current loop is obtained in this case as depicted by the black curve inserted in the field map. For the second resonance, which is split into two components (middle and rightmost figures at the top), there are three field nodes[17–19] leading in turn to two field maxima in the upper base of the SRR close to the adjacent wire. The highest field intensities are concentrated in the small space between the SRR and the wire in the case of the low-frequency component, while they are distributed among the four SRR corners in the case of the high-frequency component. Correspondingly, symmetric and antisymmetric configurations are found for the current distributions in the upper base of SRRs (black arrows in each field map). In the symmetric case (~148 THz), charge-density oscillations in the upper SRR base and nearby wire piece are in phase while they are out of phase in the antisymmetric case (~126 THz). Because the in-phase excitation leads to stronger restoring forces in the symmetric configuration,[23] the latter occurs at a higher frequency than the antisymmetric configuration. The second plasmon component mode with antisymmetric current distribution is in turn expected to disappear in the limit of touching SRRs and wires. This is confirmed in numerical simulations (Fig. 4, right). A series of new structures with touching elements was fabricated to experimentally verify the theoretical predictions (Fig. 4, top left). Results of measurements for these structures and their comparison with results obtained in the case of nontouching elements ($d=120$ nm) are presented in Fig. 4 (middle). As seen, the low-frequency component of the split mode disappears in the case of touching elements while the high-frequency component at ~150 THz, though weak, is still detected.

Field-enhancement effects in the nanoresonator/wire interspace and related field distributions were numerically investigated for the four structures of Fig. 1. Calculations were performed near the low-frequency component of the second resonance in the case of SRR-like structures with either triangular or rectangular SRRs. They were carried out near the first resonance in the case of cut-wire-like structures with

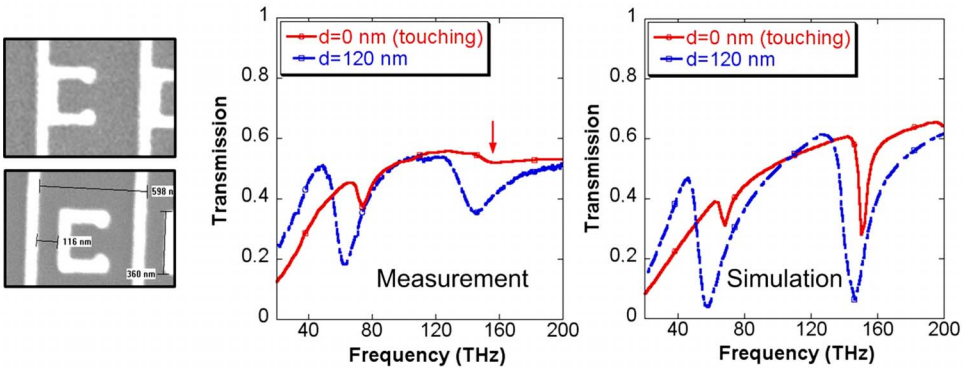

FIG. 4. (Color online) Left: micrographs of structures with touching and nontouching SRRs and wires. Middle: measured transmission spectra of the two structures. Right: numerical simulations.

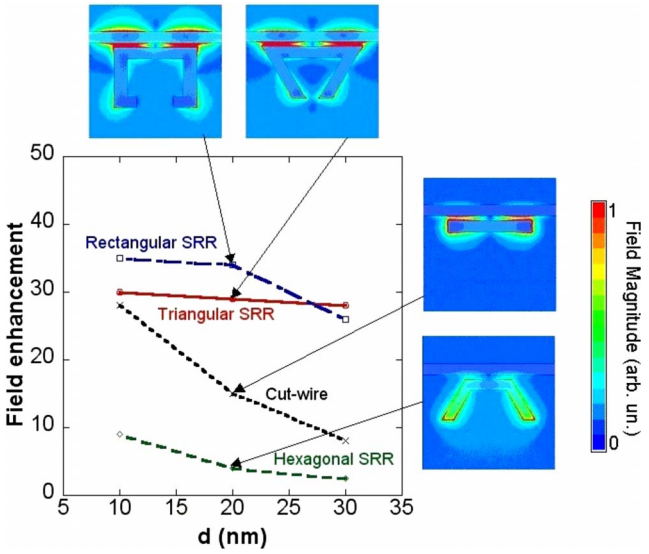

FIG. 5. (Color online) Field-enhancement factor calculated versus the distance between nanoresonators and nanowires for the four structures of Fig. 1. Calculations are performed near the low-frequency component of the second resonance in the case of SRR-like structures (triangular and rectangular SRRs). They are performed near the first resonance in the case of cut-wire-like structures (cut wires and hexagonal SRRs). Three distances are considered: $d=10$, 20, and 30 nm. Straight lines are guides for the eyes. Calculated field maps are represented for $d=20$ nm. For a given field amplitude, the same color is used in the different maps.

either cut wires or hexagonal SRRs. In each case, a very dense meshing of the structure was used for accurate finite element calculations. The mesh step size was 1 nm at the metal/silicon interface. Care was also taken to remove from the calculated results the local-field singularities occurring near sharp metallic corners. It is indeed well known that the electric field diverges at sharp metallic corners.[24] The field-enhancement factor, defined as the ratio of the local field to the incident field, typically reached 1000 at these corners. Such an enhancement is of little interest since fabricated structures necessarily have rounded corners. To suppress these artifacts, the field amplitudes were calculated for distances of at least a few nanometers from nanoresonators. Figure 5 shows the near-field-enhancement factor calculated versus the separation distance between nanoresonators and nanowires. As expected, the highest field-enhancement factors are obtained in the case of SRR-like structures. Calculated values, which lie between 30 and 40, are comparable to those recently reported by Hao *et al.*[16] for "composite ring disk cavities." It is worthwhile noting that such high enhancement factors are still obtainable for a separation distance of 30 nm, as in the experiments. Separations below 10 nm are needed to reach the same performances in the case of cut-wire structures, thus limiting the practical realization of these devices. Clearly, the different levels of field enhancement reported in Fig. 5 are in direct relation with the coupling strengths existing between the nanoresonator modes and the nanowire modes.

In summary, we have experimentally and numerically investigated properties and potential applications of infrared metamaterial layers where in-plane coupling between basic elements, i.e., metallic nanoresonators and wires, was intentionally strengthened. Not only the electromagnetic response of metamaterials can be tailored by coupling resonators and metallic wires but also strong local-field enhancement can be achieved. One major progress in this direction stems from the use of folded resonators (i.e., split ring resonators) operated near their second resonance. Because of the favorable distribution of field maxima and charges in the resonators for this resonance, strong coupling with nearby nanowires (or nanoguides) is obtained for separation distances between the two elements, which are well within the possibilities of existing e-beam lithography and metal deposition techniques. The use of the second resonance instead of the fundamental one usually involved in coupling schemes with metallic dipoles or dots also allows operating at high frequencies (or short wavelengths) despite larger feature sizes of the resonator. Strong coupling and field-enhancement effects presently reported around 120–150 THz ($\lambda=2-2.5$ μm) can be easily translated to the near infrared and visible ranges by using somewhat smaller resonators and/or dielectric substrates with a smaller index of refraction since SRR resonances have been shown to almost scale as $1/\sqrt{\varepsilon_r}$.[18] Another superiority of SRRs versus metallic dipoles or dots stems from their lower radiative losses, thus allowing in turn a more efficient excitation of guided modes through evanescent field coupling into nearby guides. Finally, the good agreement obtained between all spectroscopic measurements and numerical calculations reported in this paper shows that in-plane coupling and related effects such as resonance splittings and local-field enhancement can be controlled in a very predictable manner in optical metamaterials.

The authors wish to thank J.-J. Greffet for fruitful discussions.

*boubacar.kante@ief.u-psud.fr
†jean-michel.lourtioz@ief.u-psud.fr

[1] J. B. Pendry, A. J. Holden, D. J. Robbins, and W. J. Stewart, J. Phys.: Condens. Matter **10**, 4785 (1998).
[2] J. B. Pendry, A. J. Holden, D. J. Robbins, and W. J. Stewart, IEEE Trans. Microwave Theory Tech. **47**, 2075 (1999).
[3] D. R. Smith, W. J. Padilla, D. C. Vier, S. C. Nemat-Nasser, and S. Schultz, Phys. Rev. Lett. **84**, 4184 (2000).
[4] S. Linden, C. Enkrich, M. Wegener, J. Zhou, T. Koschny, and C. M. Soukoulis, Science **306**, 1351 (2004).
[5] G. Dolling, C. Enkrich, M. Wegener, J. F. Zhou, C. M. Soukoulis, and S. Linden, Opt. Lett. **30**, 3198 (2005).
[6] V. M. Shalaev, W. Cai, U. K. Chettiar, H. K. Yuan, A. K. Sarychev, V. P. Drachev, and A. V. Kildishev, Opt. Lett. **30**, 3356

(2005).
[7] N. Liu, H. Guo, L. Fu, S. Kaiser, H. Schweizer, and H. Giessen, Nature Mater. **7**, 31 (2008).
[8] B. Kanté, S. N. Burokur, A. Sellier, A. de Lustrac, and J.-M. Lourtioz, Phys. Rev. B **79**, 075121 (2009).
[9] J. R. Krenn, J. C. Weeber, A. Dereux, E. Bourillot, J. P. Goudonnet, B. Schider, A. Leitner, F. R. Aussenegg, and C. Girard, Phys. Rev. B **60**, 5029 (1999).
[10] C. Rockstuhl, T. Zentgraf, H. Guo, N. Liu, C. Etrich, I. Loa, K. Syassen, J. Kuhl, F. Lederer, and H. Giessen, Appl. Phys. B: Lasers Opt. **84**, 219 (2006).
[11] S. Maier and H. Atwater, J. Appl. Phys. **98**, 011101 (2005).
[12] W. L. Barnes, A. Dereux, and T. W. Ebesen, Nature (London) **424**, 824 (2003).
[13] J. N. Anker, W. P. Hall, O. Lyandres, N. C. Shah, J. Zhao, and R. P. V. Duyne, Nature Mater. **7**, 442 (2008).
[14] S. A. Maier, M. L. Brongersma, P. G. Kik, and H. A. Atwater, Phys. Rev. B **65**, 193408 (2002).
[15] A. Christ, O. J. F. Marin, Y. Ekinci, N. A. Gippius, and S. G. Tikhodeev, Nano Lett. **8**, 2171 (2008).
[16] F. Hao, Y. Sonnefraud, P. V. Dorpe, S. A. Maier, N. J. Halas, and P. Nordlander, Nano Lett. **8**, 3983 (2008).
[17] C. Rockstuhl, F. Lederer, C. Etrich, T. Zentgraf, J. Kuhl, and H. Giessen, Opt. Express **14**, 8827 (2006).
[18] B. Kanté, A. de Lustrac, J.-M. Lourtioz, and F. Gadot, Opt. Express **16**, 6774 (2008).
[19] T. Zentgraf, J. Dorfmüller, C. Rockstuhl, C. Etrich, R. Vogelgesang, K. Kern, T. Pertsch, F. Lederer, and H. Giessen, Opt. Lett. **33**, 848 (2008).
[20] J. Takahara, S. Yamagishi, H. Taki, A. Morimoto, and T. Kobayashi, Opt. Lett. **22**, 475 (1997).
[21] P. Berini, Opt. Lett. **24**, 1011 (1999).
[22] J. J. Mock, R. T. Hill, A. Degiron, S. Zauscher, A. Chilkoti, and D. R. Smith, Nano Lett. **8**, 2245 (2008).
[23] E. Prodan, C. Radloff, N. J. Halas, and P. Nordlander, Science **302**, 419 (2003).
[24] J. P. Kottmann, O. J. F. Martin, D. R. Smith, and S. Schultz, Chem. Phys. Lett. **341**, 1 (2001).